

Electronic Structure of Low-Dimensional 4d⁵ Oxides: Interplay of Ligand Distortions, Overall Lattice Anisotropy, and Spin–Orbit Interactions

Vamshi M. Katukuri,[†] Karla Roszeitis,^{†,‡} Viktor Yushankhai,^{§,||} Alexander Mitrushchenkov,[⊥] Hermann Stoll,[#] Michel van Veenendaal,^{¶,∇} Peter Fulde,^{||} Jeroen van den Brink,^{†,‡} and Liviu Hozoi^{*,†}

[†]Institute for Theoretical Solid State Physics, IFW Dresden, Helmholtzstrasse 20, 01069 Dresden, Germany

[‡]Department of Physics, Technical University Dresden, Helmholtzstrasse 10, 01069 Dresden, Germany

[§]Joint Institute for Nuclear Research, Joliot-Curie 6, 141980 Dubna, Russia

^{||}Max-Planck-Institut für Physik komplexer Systeme, Nöthnitzer Strasse 38, 01187 Dresden, Germany

[⊥]Laboratoire de Modélisation et Simulation Multi Echelle, Université Paris-Est, 5 Boulevard Descartes, 77454 Marne-la-Vallée Cedex 2, France

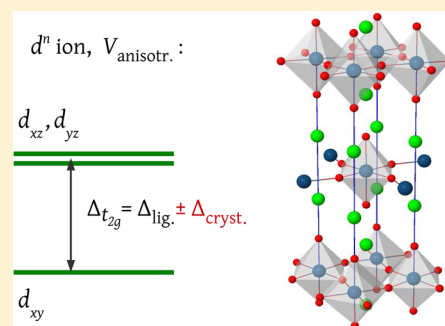
[#]Institute for Theoretical Chemistry, Universität Stuttgart, Pfaffenwaldring 55, 70550 Stuttgart, Germany

[¶]Department of Physics, Northern Illinois University, De Kalb, Illinois 60115, United States

[∇]Advanced Photon Source, Argonne National Laboratory, Argonne, Illinois 60439, United States

Supporting Information

ABSTRACT: The electronic structure of the low-dimensional 4d⁵ oxides Sr₂RhO₄ and Ca₃CoRhO₆ is herein investigated by embedded-cluster quantum chemistry calculations. A negative tetragonal-like t_{2g} splitting is computed in Sr₂RhO₄ and a negative trigonal-like splitting is predicted for Ca₃CoRhO₆, in spite of having positive tetragonal distortions in the former material and cubic oxygen octahedra in the latter. Our findings bring to the foreground the role of longer-range crystalline anisotropy in generating noncubic potentials that compete with local distortions of the ligand cage, an issue not addressed in standard textbooks on crystal-field theory. We also show that sizable t_{2g}⁵–t_{2g}⁴e_g¹ couplings via spin–orbit interactions produce in Sr₂RhO₄ ⟨Z⟩ = ⟨∑_i I_i·s_i⟩ ground-state expectation values significantly larger than 1, quite similar to theoretical and experimental data for 5d⁵ spin–orbit-driven oxides such as Sr₂IrO₄. On the other hand, in Ca₃CoRhO₆, the ⟨Z⟩ values are lower because of larger t_{2g}–e_g splittings. Future X-ray magnetic circular dichroism experiments on these 4d oxides will constitute a direct test for the ⟨Z⟩ values that we predict here, the importance of many-body t_{2g}–e_g couplings mediated by spin–orbit interactions, and the role of low-symmetry fields associated with the extended surroundings.



INTRODUCTION

One of the most difficult problems in electronic structure theory is the correct description of correlated d and f electrons in solid-state compounds. Although density functional theory (DFT) provides results in reasonably good agreement with the experiment for weakly and moderately correlated electron systems, there are many materials, in particular, d- and f-electron oxides, whose electronic structures cannot be properly treated within the canonical DFT framework. Extensions of DFT by dynamical mean-field theory (DMFT) led to DFT+DMFT schemes and allowed one to overcome some of the intrinsic limitations of DFT.^{1,2} Yet the accuracy and predictive power of the DFT+DMFT calculations is to some extent restricted by the use of parametrizations such as the on-site Coulomb repulsion *U*. It is therefore desirable to explore complementary techniques, e.g., wave-function-based quantum chemistry methods. While early attempts and the first

encouraging results go back as early as the 1970s, with the work of Wachters, Bagus, and others,^{3,4} the tremendous progress in computer technology nowadays makes possible many-body quantum chemistry calculations on larger and larger embedded clusters with remarkably good results for quantities such as the d-level splittings and intersite spin interactions; see, e.g., refs 5–34.

Most of the investigations have been focused on 3d transition-metal compounds^{3–24} and very recently, because of novel physics arising from strong spin–orbit coupling (SOC), on 5d oxides.^{25–29} The 4d materials, on the other hand, received little attention in this context. Here we investigate with the help of ab initio quantum chemistry methods the electronic structure of Sr₂RhO₄. This system is nearly isostructural with

Received: October 22, 2013

Published: April 29, 2014

the layered 3d cuprate La_2CuO_4 , one of the parent compounds of the high- T_c copper oxide superconductors,³⁵ the 4d p-wave superconductor Sr_2RuO_4 ,^{36,37} and the 5d material Sr_2IrO_4 , displaying a spin-orbit-driven Mott insulating state.^{38,39} The electronic structure of Sr_2RhO_4 was earlier addressed by both angle-resolved photoemission spectroscopy⁴⁰ and DFT calculations within the local-density approximation.^{41,42} The particular form of the Fermi surface, with no sheet of xy symmetry,⁴⁰ came as a surprise for a system with positive tetragonal distortion of the O cage around the active d-metal site (see Figure 1). It was later explained that this is the

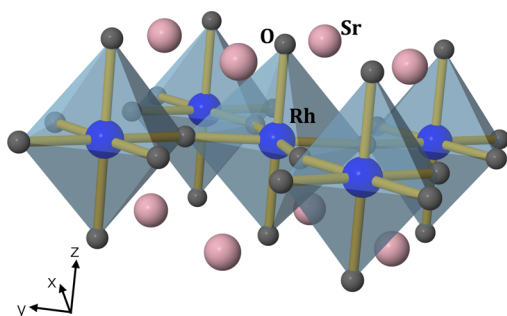


Figure 1. Layered network of corner-sharing RhO_6 octahedra in Sr_2RhO_4 . Sr sites above and below the RhO_2 planes are also shown. Two additional Sr neighbors from farther Sr layers have been included in the cluster used in the quantum chemistry calculations, lying along the apical O–Rh–O axis of the central octahedron.

outcome of the interplay of xy and $x^2 - y^2$ band mixing due to rotations of the RhO_6 octahedra, SOC, and sizable Coulomb interactions.^{41,42} We study in more detail the d-level electronic structure and find that even the *on-site* energy of the Rh xy orbital is lower than the energies of the xz and yz orbitals, despite the apical elongation of the RhO_6 octahedra, which according to basic ligand-field theory should push the xy level higher in energy;⁴³ see Figure 2. This unexpected order of the

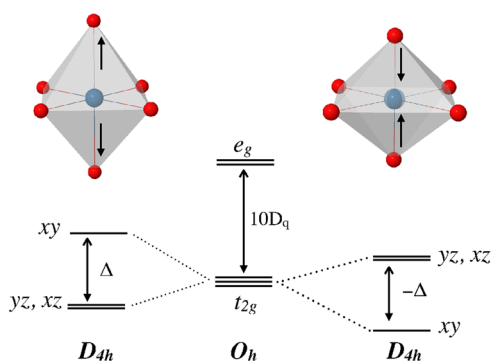


Figure 2. t_{2g} energy levels in fields of tetragonal symmetry. If the anisotropy of the extended surroundings is ignored, stretched metal–ligand bonds along the z axis raise the energy of the xy level (left), while shorter bonds along z lower the energy of the xy level (right).⁴³

Rh t_{2g} levels is the outcome of low-symmetry potentials related to the anisotropic layered structure of the extended surroundings and represents one ingredient that, in addition to the band effects discussed in refs 40–42, is important for the construction of a correct minimal effective model for Sr_2RhO_4 . A similar interplay between local distortions of the O cage and longer-range lattice anisotropy has been earlier evidenced in

trigonally distorted 5d pyrochlore oxides.^{28,29} We further compare the quantum chemistry data for the 4d t_{2g} splittings in Sr_2RhO_4 with the results for the Rh^{4+} $4d^5$ chainlike compound $\text{Ca}_3\text{CoRhO}_6$ and the 5d⁵ 214-layered materials Sr_2IrO_4 and Ba_2IrO_4 , isostructural to Sr_2RhO_4 . Negative trigonal- and tetragonal-like splittings are also found in $\text{Ca}_3\text{CoRhO}_6$ and Sr_2IrO_4 , respectively, in spite of having ideal cubic octahedra in the former compound and positive tetragonal distortions in the latter. Our study additionally addresses the effect of strong SOCs on quantities such as the ground-state (GS) expectation value of the $Z = \sum_i \mathbf{l}_i \cdot \mathbf{s}_i$ operator and the branching ratio (BR) in L-edge X-ray absorption spectroscopy (XAS). While XAS measurements are not available for Sr_2RhO_4 , the experimental trends are well reproduced in the calculations for Sr_2IrO_4 and Ba_2IrO_4 .

■ COMPUTATIONAL DETAILS

To extract the on-site d-level splittings, multiconfiguration complete-active-space self-consistent-field (CASSCF) and subsequent multireference configuration-interaction (MRCI) calculations are carried out on clusters that contain one central RhO_6 (or IrO_6) octahedron, the nearest-neighbor (NN) d-metal sites, and the nearby alkaline-earth ions, Sr, Ba, or Ca (see Figures 1 and 3). The solid-state surroundings are modeled as a large array of point charges fitted to reproduce the crystal Madelung field in the cluster region.

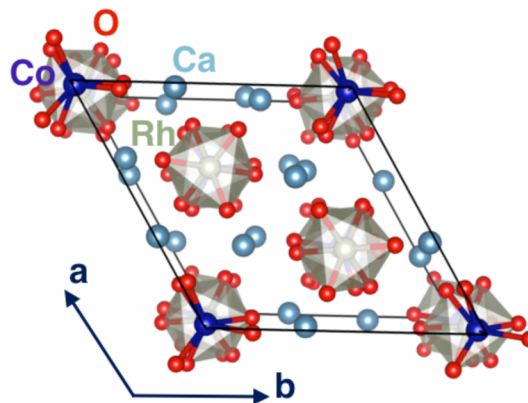


Figure 3. Crystalline structure of $\text{Ca}_3\text{CoRhO}_6$, as a projection onto the ab plane. Face-sharing RhO_6 octahedra and CoO_6 trigonal prisms form a network of quasi-one-dimensional chains along the c axis. The chainlike structure, 3-fold coordination of O NNs, and 6-fold coordination of neighboring Ca–Ca... and Rh–Co... chains give rise to effective trigonal (D_{3d}) symmetry at the d-metal sites.⁴⁸

We used energy-consistent relativistic pseudopotentials and valence basis sets of quadruple- ζ quality supplemented with f polarization functions for the central Rh^{4+} (in Sr_2RhO_4 and $\text{Ca}_3\text{CoRhO}_6$) or Ir^{4+} (in Sr_2IrO_4 and Ba_2IrO_4) ions and all-electron triple- ζ basis sets for the ligands of the central octahedron.⁴⁶ As concerns the NN d-metal sites, there are four of those in the two-dimensional square-lattice compounds Sr_2RhO_4 , Sr_2IrO_4 , and Ba_2IrO_4 (either Rh^{4+} or Ir^{4+}) and only two in the quasi-one-dimensional, chainlike compound $\text{Ca}_3\text{CoRhO}_6$ (Co^{2+}); see Figures 1 and 3 and refs 47–50. To obtain a clear picture on the effect of spin-orbit interactions at a given d⁵ site, we cut off the magnetic couplings with the adjacent d-metal ions by replacing the tetravalent open-shell d⁵ NNs with tetravalent closed-shell d⁶ species. For Sr_2RhO_4 , the

Rh⁴⁺ 4d⁵ NNs are thus replaced by Pd⁴⁺ 4d⁶ ions, while for Sr₂IrO₄ and Ba₂IrO₄, we placed at the adjacent Ir⁴⁺ 5d⁵ sites Pt⁴⁺ 5d⁶ species. We further used Zn²⁺ total-ion effective potentials⁵¹ to describe the two Co²⁺ ions next to the reference RhO₆ octahedron in Ca₃CoRhO₆. This is a usual procedure in quantum chemistry studies on transition-metal systems; see, e.g., refs 12, 25–29, and 52–54. An explicit treatment of spins at the NN d sites is technically out of the question for the calculation of quantities such as the GS expectation value of the $\mathcal{Z} = \sum_i \mathbf{l}_i \cdot \mathbf{s}_i$ operator, discussed below. We applied energy-consistent relativistic pseudopotentials and valence basis sets of triple- ζ quality for the NN 4d sites in Sr₂RhO₄⁴⁴ and for the NN 5d sites in Sr₂IrO₄ and Ba₂IrO₄⁴⁵ along with minimal atomic-natural-orbital basis sets for the additional O ions⁵⁵ coordinating those d-metal NNs.

There are 10 alkaline-earth neighboring ions in the two-dimensional square-lattice system compounds Sr₂RhO₄, Sr₂IrO₄, and Ba₂IrO₄ (see Figure 1) and 12 in the quasi-one-dimensional, chainlike compound Ca₃CoRhO₆ (see Figure 3). In each case, those Sr, Ba, or Ca species were modeled by divalent total-ion effective potentials supplemented with a single s basis function.⁵⁶ Lattice parameters as reported by Vogt and Buttrey,⁴⁷ Niitaka et al.,⁴⁸ Crawford et al.,⁴⁹ and Okabe et al.⁵⁰ were used for Sr₂RhO₄, Ca₃CoRhO₆, Sr₂IrO₄, and Ba₂IrO₄, respectively.

All computations were performed with the MOLPRO quantum chemistry software.⁵⁷ In the CASSCF calculations, only the 4d (or 5d) t_{2g} orbitals at the central Rh (or Ir) site and five electrons were included in the active space. The self-consistent-field optimization was carried out for the split ²T_{2g}(t_{2g}⁵) states.⁷⁹ All O 2p and metal t_{2g} electrons at the central octahedron were correlated in the MRCI calculations.

The spin-orbit treatment is implemented in the MOLPRO package as described in ref 58. In a first step, the scalar relativistic Hamiltonian is used to calculate correlated wave functions for the ground and a few low-lying excited states, either at the CASSCF or MRCI level. In a second step, the spin-orbit part is added to the Hamiltonian, matrix elements of the aforementioned states are evaluated for this Hamiltonian, and the resulting matrix is finally diagonalized to yield the spin-orbit-coupled states.

For Sr₂RhO₄, we analyzed in detail the sensitivity of the computed t_{2g} splittings to the way the d-metal NNs and the extended surroundings are represented. Crystalline embeddings constructed on the basis of prior Hartree-Fock calculations for the periodic lattice and the use of open-shell configurations for the NN sites were found to yield essentially the same t_{2g} splittings, in the range of 50 meV (see the Supporting Information).

RESULTS

Sr₂RhO₄. Results for the Rh t_{2g} splittings in Sr₂RhO₄ are shown in Table 1. Surprisingly, we find that the xy t_{2g} sublevel is the lowest in energy, although the apical bond lengths are

Table 1. Relative Energies (meV) for the Split Rh⁴⁺ ²T_{2g}(t_{2g}⁵) States in Sr₂RhO₄^a

hole orbital	xz/yz	xy
CASSCF	0	−50
MRCI	0	−70

^aSee the text. SOC is not included.

much larger than the in-plane Rh–O distances (2.06 vs 1.96 Å; see ref 47). Thus, the hole in the Rh t_{2g} shell has xz/yz character, in contrast to simple considerations from basic ligand-field theory for transition-metal complexes.⁴³ At the MRCI level, the splitting between the xy and xz/yz states is found to be 70 meV (see Table 1), a meaningful number compared to the 100–200 meV energy difference between the upper edges of the xy and xz/yz bands in the periodic DFT calculations.^{40,41}

The nature of the actual GS is somewhat more complex, however, because of SOCs that are important for 4d electrons. With SOC included, the spectrum of Rh t_{2g}⁵ electronic states is a sequence of three Kramers doublets (KDs).^{39,59,60} The relative energies of the MRCI Rh t_{2g}⁵ spin-orbit KDs are 0, 0.20, and 0.25 eV. In cubic symmetry, the higher states would be degenerate and define the j_{eff} = 3/2 spin-orbit quartet while the GS corresponds to the j_{eff} = 1/2 doublet.^{39,60} The j_{eff} = 1/2 to 3/2 excitation energy is directly related in cubic symmetry to the strength of the SOC ζ , $\Delta E_{1/2 \rightarrow 3/2} = 3\zeta/2$.^{60,61}

Sizable SOCs were shown to give rise to peculiar signatures in XAS. In particular, the ratio BR = I_{L₃}/I_{L₂} between the integrated intensities at the L₃ and L₂ 2p absorption edges, I_{L₃} and I_{L₂}, is directly related to the GS expectation value of the angular part of the spin-orbit operator: BR = (2 + r)/(1 − r), where r = ⟨Z⟩/⟨n_h⟩, Z = ∑_i l_i · s_i, l_i and s_i are one-electron angular momentum and spin operators, and n_h is the number of holes in the valence shell.^{62–64} For a given LS term,^{43,59}

$$\langle \mathcal{Z} \rangle = \lambda^{-1} \langle \mathcal{H}_{so} \rangle = \langle \mathbf{L} \cdot \mathbf{S} \rangle \quad (1)$$

$\mathcal{H}_{so} = \sum_i \zeta_i \mathbf{l}_i \cdot \mathbf{s}_i$ is here the spin-orbit Hamiltonian, while $\lambda = \pm \zeta/2S$ and ζ are SOC parameters for a particular dⁿ electron configuration. For less than half-filled shells, λ is positive ($\lambda = \zeta/2S$). It is negative ($\lambda = -\zeta/2S$) for more than half-filling.^{43,60} Further, for one hole in the t_{2g} shell, $\langle \mathbf{L} \cdot \mathbf{S} \rangle = -\langle \mathbf{l}_{eff} \cdot \mathbf{s} \rangle = -1/2 [j_{eff}(j_{eff} + 1) - l_{eff}(l_{eff} + 1) - S(S + 1)]$, with $S = 1/2$ and the effective quantum numbers $l_{eff} = 1$ and $j_{eff} = 1/2$.⁸⁰ It follows that, for ⟨n_h⟩ = 5, ⟨Z⟩ = 1 and BR = 2.75. Obviously, without spin-orbit interactions, BR = 2 (see also refs 62–64).

Interestingly, for 5d⁵ iridium oxides, BRs of approximately 4 and GS expectation values ⟨Z⟩ close to 2 have been derived from the XAS measurements.^{65–67} Such large values for BR and ⟨Z⟩ can only be accounted for by the sizable admixture, via SOC,^{63,64,68–71} of the leading GS configuration t_{2g}⁵ with excited-state t_{2g}⁴e_g¹ (and t_{2g}³e_g²) configurations.^{65,66}

In the presence of off-diagonal SOCs, ⟨Z⟩ is most conveniently expressed as^{63,64}

$$\langle \mathcal{Z} \rangle = \zeta^{-1} (E_{LS}^0 - E_{LSJ}^0) \quad (2)$$

where E_{LS}⁰ is the energy of the lowest dⁿ state without spin-orbit treatment and E_{LSJ}⁰ is the GS eigenvalue with spin-orbit interactions accounted for. Spin-orbit matrix elements have been tabulated for the octahedral d⁵ manifold by Schroeder⁶⁸ and the effect of off-diagonal spin-orbit interactions for, e.g., Ir⁴⁺ 5d⁵ ions anticipated already a few decades ago by Thornley, Allen, and Andlauer et al.^{69–71}

⟨Z⟩ GS expectation values are listed for the Rh⁴⁺ 4d⁵ electron configuration of Sr₂RhO₄ in Table 2, for different active spaces. Such expectation values are easily derived using eq 2 and the eigenvalues provided by MOLPRO for the ²T_{2g}(t_{2g}⁵) configuration state function and for the many-body

Table 2. $\langle Z \rangle = \langle \sum_i I_i \cdot s_i \rangle$ for the Rh⁴⁺ 4d⁵ ion in Sr₂RhO₄^a

no. of states	CASSCF	MRCI
1D (3 KDs with SOC)	0.89	
1D, 2Q, 1S (18 KDs)	1.29	1.17
5D, 2Q, 1S (27 KDs)	1.37	1.24 ^b
9D, 8Q, 1S (60 KDs)	1.38	

^aSee the text. The number of states included in the spin-orbit treatment, i.e., doublets (D), quartets (Q), and sextets (S), is given in the left column. The separation between the lowest t_{2g}^5 and $t_{2g}^4 e_g^1$ states is 1.96 eV by MRCI. ^bThe weight of the $t_{2g}^4 e_g^1$ and $t_{2g}^3 e_g^2$ configurations in the GS wave function is 3%.

spin-orbit GS. Because the SOC constant ζ is not directly provided in *MOLPRO*, we extract this parameter by mapping the ab initio energies of the spin-orbit components arising from the ${}^2T_{2g}(t_{2g}^5)$ term onto the eigenvalues associated with the spin-orbit matrix elements tabulated in, e.g., ref 68. To this end, we carry out a set of additional quantum chemistry calculations for the hypothetical cubic perovskite CaRhO₃; see the Supporting Information. Although matrix elements for the case of tetragonal distortions were earlier tabulated for various d⁵ states by Goode,⁷² we avoid in this way all complications associated with the lower point-group symmetry in Sr₂RhO₄. The outcome of the calculations on the idealized cubic perovskite structure is a SOC $\zeta = 0.147$ eV; see the Supporting Information.

If the active orbital space in the CASSCF calculation is restricted to the three Rh t_{2g} orbitals, $\langle Z \rangle$ is indeed approximately 1, in fact somewhat lower than 1 because of the splitting of the t_{2g} levels; see the first line in Table 2 and the Supporting Information. When the active space is enlarged with Rh e_g orbitals, $\langle Z \rangle$ dramatically increases, although the weight of the $t_{2g}^4 e_g^1$ and $t_{2g}^3 e_g^2$ configurations in the spin-orbit GS wave function is not larger than 3%. We first included in the spin-orbit treatment the split ${}^2T_{2g}$ related to the t_{2g}^5 configuration and additionally the (split) ${}^4T_{1g}(t_{2g}^4 e_g^1)$, ${}^4T_{2g}(t_{2g}^4 e_g^1)$, and ${}^6A_{1g}(t_{2g}^3 e_g^2)$ components. The orbitals were optimized for an average of all of these terms.⁸¹ The results from such spin-orbit calculations are listed on the second line in Table 2. The doublet, quartet, and sextet states that enter the spin-orbit treatment are labeled as D, Q, and S, respectively. For the results on the third line in Table 2, we further added to the spin-orbit calculation the low-lying ${}^2A_{2g}$, ${}^2T_{1g}$, 2E_g , and ${}^2T_{2g}$ components arising from the $t_{2g}^4 e_g^1$ manifold. Calculations with even more excited states in the spin-orbit treatment (see the lowest line in Table 2) show that the $\langle Z \rangle$ GS expectation values are pretty much converged. For the latter set of results, the MRCI spin-orbit calculation is too expensive and only the CASSCF+SOC $\langle Z \rangle$ value is shown. All quartet $t_{2g}^4 e_g^1({}^4T_{1g}, {}^4T_{2g})$ and $t_{2g}^3 e_g^2({}^4A_{1g}, {}^2E_g, {}^4T_{2g}, {}^4T_{1g}, {}^4A_{2g})$ and doublet $t_{2g}^4 e_g^1({}^2A_{2g}, {}^2T_{1g}, {}^2E_g, {}^2T_{2g}, {}^2A_{1g})$ components are here included in the spin-orbit treatment.

The values computed with the larger active spaces in Table 2 are actually not very much off the values derived from the L-edge XAS spectra of Ir⁴⁺ 5d⁵ oxides.^{65–67} Although the SOC is substantially lower for 4d ions, the $t_{2g}-e_g$ octahedral crystal-field splitting is also smaller for 4d electrons. This is due to the more compact nature of the 4d orbitals compared to the 5d functions. From CASSCF to MRCI, the $t_{2g}-e_g$ splitting is slightly enhanced⁸² and therefore $\langle Z \rangle$ is somewhat reduced. To

restrict the configurational space to the t_{2g}^5 manifold alone, only the CASSCF $\langle Z \rangle$ value is given on the first line in Table 2.

Model Hamiltonian calculations of the dichroic XAS spectra show that fine details such as the integrated intensities at the L₂ and L₃ edges depend on how the hole in the t_{2g} shell is distributed over the three t_{2g} components.⁶⁶ A lower energy of the xy level yields larger hole density in the xz and yz orbitals in the spin-orbit GS wave function. Our findings for the relative energies of the Rh t_{2g} orbitals can therefore, in principle, be verified by high-resolution XAS and X-ray magnetic circular dichroism (XMCD) measurements. Optical absorption or resonant inelastic X-ray scattering cannot provide direct evidence for the relative order of the 4d or 5d t_{2g} levels because of the strong admixture of the three different t_{2g} components in the spin-orbit wave functions.

Ca₃CoRhO₆. L-edge XAS spectra are presently available for Rh⁴⁺ 4d⁵ ions in Ca₃CoRhO₆⁷³ and indicate BRs close to 2 and $\langle Z \rangle$ GS expectation values rather close to 1. MRCI spin-orbit calculations for the Rh⁴⁺ 4d⁵ configuration in the rhodium oxide compound Ca₃CoRhO₆ yield GS expectation values $\langle Z \rangle \approx 1.1$ (see Table 3), indeed lower than $\langle Z \rangle \approx 1.25$ in Sr₂RhO₄ (Table 2). Electron itineracy might further reduce somewhat these $\langle Z \rangle$ GS expectation values.

Table 3. $\langle Z \rangle$ Values for the Rh⁴⁺ 4d⁵ Ion in Ca₃CoRhO₆ When GS Wave Functions of Increasing Quality Are Used^a

no. of states	CASSCF	MRCI
1D (3 KDs with SOC)	0.84	
1D, 2Q, 1S (18 KDs)	1.16	1.05
5D, 2Q, 1S (27 KDs)	1.21	1.09
9D, 8Q, 1S (60 KDs)	1.23	

^aThe CASSCF and MRCI calculations are carried out similarly to the results in Table 2. The MRCI t_{2g} splitting is 0.10 eV and the separation between the lowest t_{2g}^5 and $t_{2g}^4 e_g^1$ states is 2.61 eV.

Our analysis suggests that the difference between the $\langle Z \rangle$ GS expectation values in Ca₃CoRhO₆ and Sr₂RhO₄ is related to the larger separation between the lowest t_{2g}^5 and $t_{2g}^4 e_g^1$ states, i.e., 2.61 eV in Ca₃CoRhO₆ versus 1.96 eV in Sr₂RhO₄, and to a smaller extent to the slightly larger Rh t_{2g} splitting in Ca₃CoRhO₆. The Rh t_{2g} levels are split up in Ca₃CoRhO₆ as well, in spite of the perfect RhO₆ octahedra.⁴⁸ This is again related to anisotropic fields, of trigonal symmetry in Ca₃CoRhO₆,⁴⁸ generated by the extended surroundings. That the point-group symmetry at the Rh sites is D_{3d} lower than O_h is apparent from Figure 3. It has to do with the quasi-one-dimensional structure, 3-fold coordination of O NNs, and 6-fold coordination of neighboring Ca–Ca... and Rh–Co... chains.

Similar findings, of finite t_{2g} splittings, have been reported for Ir⁴⁺ 5d⁵ ions with perfect octahedral O cages in the pyrochlore structure.²⁸ For the trigonal setting in Ca₃CoRhO₆,⁴⁸ the ab initio results show that the a_{1g} sublevel is lower in energy than the e_g' sublevels,⁸³ by 0.10 eV in MRCI. The sequence that we find in the quantum chemistry calculations for the Rh t_{2g} states can be, in principle, verified by careful analysis of future XMCD spectra.

A further interesting observation with respect to the data in Table 3 is that, even if the $t_{2g}^5-t_{2g}^4 e_g^1$ couplings are strong, the result of these spin-orbit-mediated interactions on $\langle Z \rangle$ may be drastically diminished because of the presence of low-

symmetry, noncubic fields. The latter mix the $t_{2g}^5 j_{\text{eff}} = 1/2$ and $3/2$ components (see the Supporting Information) and this effect is stronger in 4d compounds, where the SOC ζ is not very much different from the typical values of the t_{2g} splittings.

Sr₂IrO₄ AND Ba₂IrO₄. In the local-density approximation to DFT, the band structures of Sr₂IrO₄ and Sr₂RhO₄ are quite similar around the Fermi level.^{39,40} To put the results on Sr₂RhO₄ into perspective, we provide in this section CASSCF and MRCI data for the Ir d-level splittings and $\langle Z \rangle$ GS expectation values in Sr₂IrO₄ and Ba₂IrO₄, structurally closely related to Sr₂RhO₄.^{47,49,50} Ir t_{2g} splittings are listed in Table 4,

Table 4. Relative Energies (meV) for the Split Ir $^2T_{2g}(t_{2g}^5)$ States in Sr₂IrO₄ and Ba₂IrO₄^a

hole orbital	xz/yz	xy
Sr ₂ IrO ₄		
CASSCF	0	-120
MRCI	0	-155
Ba ₂ IrO ₄		
CASSCF	0	70
MRCI	0	65

^aSOC is not accounted for.

Table 5. $\langle Z \rangle$ GS Expectation Values for the Ir⁴⁺ 5d⁵ Ion in Sr₂IrO₄^a

no. of states	CASSCF	MRCI
1D (3 KDs with SOC)	0.92	
1D, 2Q, 1S (18 KDs)	1.56	1.46
5D, 2Q, 1S (27 KDs)	1.78	1.66 ^b
9D, 8Q, 1S (60 KDs)	1.82	

^aThe CASSCF and MRCI calculations are carried out similarly to the results in Table 2. The separation between the lowest t_{2g}^5 and $t_{2g}^4 e_g^1$ states is 2.59 eV by MRCI. ^bThe weight of the $t_{2g}^4 e_g^1$ and $t_{2g}^3 e_g^2$ configurations in the GS wave function is 6%.

Table 6. $\langle Z \rangle$ GS Expectation Values for the Ir⁴⁺ 5d⁵ Ion in Ba₂IrO₄^a

no. of states	CASSCF	MRCI
1D (3 KDs with SOC)	0.91	
1D, 2Q, 1S (18 KDs)	1.63	1.54
5D, 2Q, 1S (27 KDs)	1.86	1.76 ^b
9D, 8Q, 1S (60 KDs)	1.91	

^aThe CASSCF and MRCI calculations are carried out similarly to the results in Table 2. The separation between the lowest t_{2g}^5 and $t_{2g}^4 e_g^1$ states is 2.07 eV by MRCI. ^bThe weight of the $t_{2g}^4 e_g^1$ and $t_{2g}^3 e_g^2$ configurations in the GS wave function is 10%.

while $\langle Z \rangle$ values are collected in Tables 5 and 6. To compute the data in Tables 5 and 6, we used eq 2 and a SOC $\zeta = 0.468$ eV corresponding to a hypothetical cubic perovskite, CaIrO₃, having the Ir–O bond length obtained as a weighted average over the Ir–O bond lengths in Sr₂IrO₄ and Ba₂IrO₄.^{49,50} see also the Supporting Information.

The difference between the apical and in-plane metal–oxygen bond lengths is very similar for oxygen octahedra in Sr₂IrO₄ and Sr₂RhO₄, i.e., 2.06 versus 1.98 Å in Sr₂IrO₄ and 2.06 versus 1.96 Å in Sr₂RhO₄.^{47,49} Also for Sr₂IrO₄, the calculations show that the xy orbital is lower in energy than xz

and yz (see the upper half of Table 4). In Ba₂IrO₄, the stretching of the apical bonds is much stronger, with an apical Ir–O bond length of 2.15 Å.⁵⁰ For the latter material, this stronger tetragonal distortion finally pulls the xy level above xz and yz ; see the lower half of Table 4, as expected in canonical ligand-field theory.

The $\langle Z \rangle$ values listed for Sr₂IrO₄ on the lower lines in Table 5, $\langle Z \rangle = 1.7/1.8$, are comparable with a result of 2.1 extracted from XAS/XMCD data.⁶⁶ At the same level of theory, $\langle Z \rangle$ is slightly higher in Ba₂IrO₄, $\langle Z \rangle = 1.8/1.9$ (see Table 6), which reproduces the trend found in the XAS/XMCD measurements.^{66,67} The difference between the $\langle Z \rangle$ GS expectation values in the two compounds mainly comes from the different $t_{2g}-e_g$ energy separation, with t_{2g}^5 to $t_{2g}^4 e_g^1$ excitation energies lower by 0.5 eV in Ba₂IrO₄ (see the captions of Tables 5 and 6).

CONCLUSIONS

In summary, we investigated the d-level electronic structure of Sr₂RhO₄, a prototype 4d-electron oxide,^{36,37,40–42} and of the low-dimensional system Ca₃CoRhO₆. In particular, we addressed the interplay between local distortions of the O cage and longer-range lattice anisotropy and showed that the latter may actually give rise to, e.g., negative tetragonal-like splittings even for stretched apical metal–oxygen bonds, i.e., positive tetragonal distortions. Such findings are at odds with predictions from basic ligand-field theory for transition-metal complexes. Our results are relevant in connection to, e.g., angle-resolved photoemission measurements on Sr₂RhO₄ that evidence no states of xy symmetry at the Fermi level,⁴⁰ but have implications beyond this particular material. A similar interplay has been recently revealed in pyrochlore 5d oxides^{28,29} and points to the high sensitivity of the more extended 4d and 5d functions to how the anisotropic crystalline fields vary along different directions in space.

Also for the isostructural 5d⁵ material Sr₂IrO₄, having bond lengths nearly identical with that of Sr₂RhO₄,^{47,49} detailed analysis of the XAS and XMCD spectra shows a larger hole density in the xz/yz orbitals⁶⁶ and supports a negative tetragonal splitting. A negative tetragonal splitting in Sr₂IrO₄ has also been inferred from recent nonresonant magnetic X-ray diffraction experiments.⁷⁴ Interesting in this context would be detailed quantum chemistry investigations of the 4d t_{2g} splittings and interactions in Li₂RhO₃, a proposed realization of the Kitaev spin model,⁷⁵ and in 4d⁴ compounds such as the p-wave superconductor Sr₂RuO₄^{36,37} and the Mott insulator Ca₂RuO₄.^{76,77}

We further analyzed the role of $t_{2g}-e_g$ many-body couplings mediated by spin–orbit interactions and showed that in Sr₂RhO₄ they give rise to effects such as those evidenced by XAS and XMCD measurements on the 5d⁵ compounds Sr₂IrO₄ and Ba₂IrO₄,^{66,67} i.e., sizable deviations from the canonical $\langle Z \rangle = 1$ picture for a “pure” $j_{\text{eff}} = 1/2$ system.^{39,60} The experimental trend, with a $\langle Z \rangle$ GS expectation value that for Ba₂IrO₄ is larger than for Sr₂IrO₄, is reproduced in the ab initio calculations and assigned to the smaller $t_{2g}-e_g$ splitting in Ba₂IrO₄.

ASSOCIATED CONTENT

Supporting Information

Computation of the SOC constants, reduction of $\langle Z \rangle$ due to distortions in the simplified j_{eff} picture, dependence of the Rh t_{2g} splittings on details of the embedding scheme, and a table of

relative energies. This material is available free of charge via the Internet at <http://pubs.acs.org>.

AUTHOR INFORMATION

Corresponding Author

*E-mail: lhozoi@ifw-dresden.de.

Notes

The authors declare no competing financial interest.

ACKNOWLEDGMENTS

This article is dedicated to Prof. Ria Broer to honor her devoted career in Theoretical and Computational Chemistry. We thank N. A. Bogdanov and K. Koepernik for useful discussions. L.H. acknowledges financial support from the German Research Foundation (Deutsche Forschungsgemeinschaft).

REFERENCES

- (1) Georges, A.; Kotliar, G.; Krauth, W.; Rozenberg, M. J. *Rev. Mod. Phys.* **1996**, *68*, 13.
- (2) Maier, T.; Jarrell, M.; Pruschke, T.; Hettler, M. H. *Rev. Mod. Phys.* **2005**, *77*, 1027.
- (3) Wachters, A. J. H.; Nieuwpoort, W. C. *Phys. Rev. B* **1972**, *5*, 4291.
- (4) Bagus, P. S.; Freeman, A. J.; Sasaki, F. *Phys. Rev. Lett.* **1973**, *30*, 850.
- (5) Janssen, G. J. M.; Nieuwpoort, W. C. *Phys. Rev. B* **1988**, *38*, 3449.
- (6) Barandiarán, Z.; Seijo, L. J. *Chem. Phys.* **1988**, *89*, 5739.
- (7) Martin, R. L. J. *Chem. Phys.* **1993**, *98*, 8691.
- (8) Doll, K.; Dolg, M.; Fulde, P.; Stoll, H. *Phys. Rev. B* **1997**, *55*, 10282.
- (9) Bagus, P. S.; Broer, R.; de Graaf, C.; Nieuwpoort, W. C. *J. Electron Spectrosc.* **1999**, *98–99*, 303.
- (10) Muñoz, D.; Illas, F.; de P. R. Moreira, I. *Phys. Rev. Lett.* **2000**, *84*, 1579.
- (11) Muñoz, D.; de Graaf, C.; Illas, F. J. *Comput. Chem.* **2004**, *25*, 1234.
- (12) Hozoi, L.; de Vries, A. H.; van Oosten, A. B.; Broer, R.; Cabrero, J.; de Graaf, C. *Phys. Rev. Lett.* **2002**, *89*, 076407.
- (13) Suaud, N.; Lepetit, M.-B. *Phys. Rev. Lett.* **2002**, *88*, 056405.
- (14) Hozoi, L.; Laad, M. S. *Phys. Rev. Lett.* **2007**, *99*, 256404.
- (15) Sadoc, A.; Broer, R.; de Graaf, C. *J. Chem. Phys.* **2007**, *126*, 134709.
- (16) Landron, S.; Soret, J.; Lepetit, M. B. *J. Phys.: Condens. Matter* **2012**, *22*, 345603.
- (17) Hozoi, L.; Fulde, P. *Phys. Rev. Lett.* **2009**, *102*, 136405.
- (18) Hozoi, L.; Siurakshina, L.; Fulde, P.; van den Brink, J. *Sci. Rep.* **2011**, *1*, 65.
- (19) Stoyanova, A.; Hozoi, L.; Fulde, P.; Stoll, H. *Phys. Rev. B* **2011**, *83*, 205119.
- (20) de Lara-Castells, M. P.; Mitrushchenkov, A. O. *J. Phys. Chem. C* **2011**, *115*, 17540.
- (21) Domingo, A.; Rodríguez-Fortea, A.; Swart, M.; de Graaf, C.; Broer, R. *Phys. Rev. B* **2012**, *85*, 155143.
- (22) Kanan, D. K.; Carter, E. A. *J. Phys. Chem. C* **2013**, *117*, 13816.
- (23) Pradipto, A. M.; Maurice, R.; Guihéry, N.; de Graaf, C.; Broer, R. *Phys. Rev. B* **2012**, *85*, 014409.
- (24) Maurice, R.; Pradipto, A.-M.; de Graaf, C.; Broer, R. *Phys. Rev. B* **2012**, *86*, 024411.
- (25) Katukuri, V. M.; Stoll, H.; van den Brink, J.; Hozoi, L. *Phys. Rev. B* **2012**, *85*, 220402.
- (26) Bogdanov, N. A.; Katukuri, V. M.; Stoll, H.; van den Brink, J.; Hozoi, L. *Phys. Rev. B* **2012**, *85*, 235147.
- (27) Katukuri, V. M.; Nishimoto, S.; Yushankhai, V.; Stoyanova, A.; Kandpal, H.; Choi, S. K.; Coldea, R.; Roussochatzakis, I.; Hozoi, L.; van den Brink, J. *New J. Phys.* **2014**, *16*, 013056.
- (28) Hozoi, L.; Gretarsson, H.; Clancy, J. P.; Jeon, B.-G.; Lee, B.; Kim, K. H.; Yushankhai, V.; Fulde, P.; Kim, Y.-J.; van den Brink, J. *J. Phys. Rev. B* **2014**, *89*, 115111.
- (29) Bogdanov, N. A.; Maurice, R.; Roussochatzakis, I.; van den Brink, J.; Hozoi, L. *Phys. Rev. Lett.* **2013**, *110*, 127206.
- (30) Barandiarán, Z.; Seijo, L. *J. Chem. Phys.* **2013**, *138*, 074102.
- (31) Huang, P.; Carter, E. A. *Annu. Rev. Phys. Chem.* **2008**, *59*, 261.
- (32) Hozoi, L.; Fulde, P. *Computational Methods for Large Systems: Electronic Structure Approaches for Biotechnology and Nanotechnology*; John Wiley & Sons: Hoboken, NJ, 2011.
- (33) Müller, C.; Paulus, B. *Phys. Chem. Phys.* **2012**, *14*, 7605.
- (34) Sousa, C.; Tosoni, S.; Illas, F. *Chem. Rev.* **2013**, *113*, 4456.
- (35) Bednorz, J. G.; Müller, K. A. *Z. Phys. B* **1986**, *64*, 189.
- (36) Mackenzie, A. P.; Maeno, Y. *Rev. Mod. Phys.* **2003**, *75*, 657.
- (37) Maeno, Y.; Kittaka, S.; Nomura, T.; Yonezawa, S.; Ishida, K. *J. Phys. Soc. Jpn.* **2012**, *81*, 011009.
- (38) Kim, B. J.; Ohsumi, H.; Komesu, T.; Sakai, S.; Morita, T.; Takagi, H.; Arima, T. *Science* **2009**, *323*, 1329.
- (39) Kim, B. J.; Jin, H.; Moon, S. J.; Kim, J.-Y.; Park, B.-G.; Leem, C. S.; Yu, J.; Noh, T. W.; Kim, C.; Oh, S.-J.; et al. *Phys. Rev. Lett.* **2008**, *101*, 076402.
- (40) Kim, B. J.; Yu, J.; Koh, H.; Nagai, I.; Ikeda, S. I.; Oh, S.-J.; Kim, C. *Phys. Rev. Lett.* **2006**, *97*, 106401.
- (41) Liu, G. Q.; Antonov, V. N.; Jepsen, O.; Andersen, O. K. *Phys. Rev. Lett.* **2008**, *101*, 026408.
- (42) Haverkort, M. W.; Elfimov, I. S.; Tjeng, L. H.; Sawatzky, G. A.; Damascelli, A. *Phys. Rev. Lett.* **2008**, *101*, 026406.
- (43) Ballhausen, C. J. *Introduction to Ligand Field Theory*; McGraw-Hill: New York, 1962.
- (44) Peterson, K. A.; Figgen, D.; Dolg, M.; Stoll, H. *J. Chem. Phys.* **2007**, *126*, 124101.
- (45) Figgen, D.; Peterson, K. A.; Dolg, M.; Stoll, H. *J. Chem. Phys.* **2009**, *130*, 164108.
- (46) Dunning, T. H. *J. Chem. Phys.* **1989**, *90*, 1007.
- (47) Vogt, T.; Buttrey, D. J. *J. Solid State Chem.* **1996**, *123*, 186.
- (48) Niitaka, S.; Kageyama, H.; Kato, M.; Yoshimura, K.; Kosuge, K. *J. Solid State Chem.* **1999**, *146*, 137.
- (49) Crawford, M. K.; Subramanian, M. A.; Harlow, R. L.; Fernandez-Baca, J. A.; Wang, Z. R.; Johnston, D. C. *Phys. Rev. B* **1994**, *49*, 9198.
- (50) Okabe, H.; Isobe, M.; Takayama-Muromachi, E.; Koda, A.; Takeshita, S.; Hiraishi, M.; Miyazaki, M.; Kadono, R.; Miyake, Y.; Akimitsu, J. *Phys. Rev. B* **2011**, *83*, 155118.
- (51) Igel-Mann, G. Ph.D. Thesis, University of Stuttgart, Stuttgart, Germany, 1987.
- (52) de Graaf, C.; Sousa, C.; Broer, R. *J. Mol. Struct.* **1999**, *458*, 53.
- (53) Huang, H.-Y.; Bogdanov, N. A.; Siurakshina, L.; Fulde, P.; van den Brink, J.; Hozoi, L. *Phys. Rev. B* **2011**, *84*, 235125.
- (54) Maurice, R.; Verma, P.; Zdrozny, J. M.; Luo, S.; Borycz, J.; Long, J. R.; Truhlar, D. G.; Gagliardi, L. *Inorg. Chem.* **2013**, *52*, 9379.
- (55) Pierloot, K.; Dumez, B.; Widmark, P.-O.; Roos, B. *Theor. Chim. Acta* **1995**, *90*, 87.
- (56) Fuentealba, P.; von Szentpály, L.; Preuss, H.; Stoll, H. *J. Phys. B* **1985**, *18*, 1287.
- (57) Werner, H.-J.; Knowles, P. J.; Knizia, G.; Manby, F. R.; Schütz, M. *MOLPRO*; University of Cardiff: Cardiff, U.K., 2012; <http://www.molpro.net>.
- (58) Berning, A.; Schweizer, M.; Werner, H.-J.; Knowles, P. J.; Palmieri, P. *Mol. Phys.* **2000**, *98*, 1823.
- (59) Griffith, J. S. *The Theory of Transition-Metal Ions*, 5th ed.; Cambridge University Press: Cambridge, U.K., 2009.
- (60) Abragam, A.; Bleaney, B. *Electron Paramagnetic Resonance of Transition Ions*; Clarendon Press: Oxford, U.K., 1970.
- (61) Kim, J.; Casa, D.; Upton, M. H.; Gog, T.; Kim, Y.-J.; Mitchell, J. F.; van Veenendaal, M.; Daghofer, M.; van den Brink, J.; Khaliullin, G.; et al. *Phys. Rev. Lett.* **2012**, *108*, 177003.
- (62) Thole, B. T.; van der Laan, G. *Phys. Rev. A* **1988a**, *38*, 1943.
- (63) Thole, B. T.; van der Laan, G. *Phys. Rev. B* **1988b**, *38*, 3158.
- (64) van der Laan, G. *Phys. Scr.* **1990**, *41*, 574.
- (65) Laguna-Marco, M. A.; Haskel, D.; Souza-Neto, N.; Lang, J. C.; Krishnamurthy, V. V.; Chikara, S.; Cao, G.; van Veenendaal, M. *Phys. Rev. Lett.* **2010**, *105*, 216407.

(66) Haskel, D.; Fabbris, G.; Zhernenkov, M.; Kong, P. P.; Jin, C.; Cao, G.; van Veenendaal, M. *Phys. Rev. Lett.* **2012**, *109*, 027204.

(67) Boseggia, S.; Springell, R.; Walker, H. C.; Rønnow, H. M.; Rüegg, C.; Okabe, H.; Isobe, M.; Perry, R. S.; Collins, S. P.; McMorrow, D. F. *Phys. Rev. Lett.* **2013**, *110*, 117207.

(68) Schroeder, K. A. *J. Chem. Phys.* **1962**, *37*, 1587.

(69) Thornley, J. H. M. *J. Phys. C (Proc. Phys. Soc.)* **1968**, *1*, 1024.

(70) Allen, G. C.; Al-Mobarak, R.; El-Sharkawi, G. A. M.; Warren, K. D. *Inorg. Chem.* **1972**, *11*, 787.

(71) Andlauer, B.; Schneider, J.; Tolksdorf, W. *Phys. Status Solidi B* **1976**, *73*, 533.

(72) Goode, D. H. *J. Chem. Phys.* **1965**, *43*, 2830.

(73) Burnus, T.; Hu, Z.; Wu, H.; Cezar, J. C.; Niitaka, S.; Takagi, H.; Chang, C. F.; Brookes, N. B.; Lin, H.-J.; Jang, L. Y.; et al. *Phys. Rev. B* **2008**, *77*, 205111.

(74) Fujiyama, S.; Ohsumi, H.; Ohashi, K.; Hirai, D.; Kim, B. J.; Arima, T.; Takata, M.; Takagi, H., arXiv:1308.0923 (unpublished).

(75) Luo, Y.; Cao, C.; Si, B.; Li, Y.; Bao, J.; Guo, H.; Yang, X.; Shen, C.; Feng, C.; Dai, J.; et al. *Phys. Rev. B* **2013**, *87*, 161121.

(76) Gorelov, E.; Karolak, M.; Wehling, T. O.; Lechermann, F.; Lichtenstein, A. I.; Pavarini, E. *Phys. Rev. Lett.* **2010**, *104*, 226401.

(77) Liu, G.-Q. *Phys. Rev. B* **2013**, *88*, 104428.

(78) Abragam, A.; Price, M. H. L. *Proc. R. Soc. A* **1951**, *205*, 135.

(79) Although the actual point-group symmetry is lower than octahedral, we still use throughout the paper the more convenient notations corresponding to O_h symmetry.

(80) The $l_{\text{eff}} = 1$ nomenclature is extensively used in the literature. It maps the problem of t_{2g} d functions onto that of p functions. It is based on an idea of Abragam and Price⁷⁸ and is also referred to as the fictitious $\tilde{l} = 1$ angular momentum (see Chapter 7.5 in ref 60) or the t^n-p^n isomorphism (see Chapter 9.5 in ref 59). Within the t_{2g} representation, the d functions transform into each other under the angular momentum operators as do p functions, up to a factor of -1 , such that $L = -l_{\text{eff}}$ ^{59,60}

(81) Inclusion of the ${}^6A_{1g}$ state in the CASSCF optimization ensures quick convergence.

(82) In MRCI, the O 2p to metal d charge-transfer-type excitations stabilize the t_{2g}^5 states, with no charge in the metal e_g shell.

(83) $T_{2g}(O_h) \rightarrow A_{1g} + E_g(D_{3d})$ and $E_g(O_h) \rightarrow E_g(D_{3d})$. The e_g' notation is extensively used for those d states of e_g symmetry in D_{3d} originating from the states of t_{2g} symmetry in O_h .